ULTRASONIC IMAGING 16, 265-287 (1994)

ULTRASOUND ECHO ENVELOPE ANALYSIS USING A HOMODYNED K DISTRIBUTION SIGNAL MODEL

Vinayak Dutt and James F. Greenleaf

Biodynamics Research Unit
Department of Physiology and Biophysics
Mayo Graduate School
Rochester MN 55905

The statistics of ultrasound echo envelope signals can be used to characterize scattering media. The Rayleigh distribution and its generalized forms, the K and Rice distributions, have been previously used to model the echo signal. A more generalized statistical model, the homodyned K distribution, combines the K and Rice distribution features to better account for the statistics of the echo signal. We show that this model can give two parameters that are useful for media characterization: k, the ratio of coherent to diffuse signals, and, β, which characterizes the clustering of scatterers in the medium.

Key words: Echo envelope statistics modeling; homodyned K distribution.

1. INTRODUCTION

The echo signal in medical ultrasound imaging has a statistical nature arising out of interference of signals from a large number of randomly distributed scatterers. The statistics of this signal can be used for tissue characterization. In the case of large numbers of such unresolved randomly distributed scatterers, the distribution of the echo envelope has a Rayleigh distribution and the speckle pattern is normally called "fully developed" speckle [1–4]. In such a case, the only useful information carried by the signal is the mean backscattered energy. The second order statistics, autocorrelation function and the spectrum of the echo (rf) signal have been used to estimate the scatterer size, assuming a certain model for scattering by a single scatterer [4]. Using broadband signals, spectral characteristics of echo signals [5] have been obtained for tissue characterization in such Rayleigh distribution modeling scattering regimes. But the Rayleigh distribution model, or a "fully developed" speckle is not necessarily the norm in echo imaging. First, the number of scatterers may not be large enough. Second, the scatterers may not be randomly located (there may be periodicity or clustering in the spatial distribution of scatterers) or the signal may have an offset due to the "structure" (unresolved and resolved periodicity in scatterer locations) in scatterers or scattering sites. This makes the statistics of the echo envelope non-Rayleigh in general. Previously, the Rice distribution has been suggested as accounting for such deviations from the Rayleigh distribution [1,4,6]. The K distribution has also been suggested to account for clustering (i.e., nonuniform distribution) of scatterers or small numbers of scatterers [7–10]. In our approach, we use a combination of the above two meth-

0161-7346/94 $6.00

ods, a hybrid model for the statistics, namely the homodyned K distribution, which has been earlier suggested for the statistics of laser speckle in turbulent media by Jakeman [7]. This model, though of higher complexity than either the Rice or the K distribution models, gives more information about the statistics of the envelope signal. From the model paramaters two parameters are derived: k, the ratio of coherent to diffuse signals, and, β, the parameter characterizing the clustering of scatterers, and also the effective number of scatterers as suggested by Jakeman [11]). These signal amplitude independent parameters may be used to characterize the media. The purpose of this paper is to illustrate with simulations and data from phantoms that the homodyned K distribution provides parameters that extend the applicability of statistical models to a wider range of scatterer densities and distributions. We first summarize the various statistical distribution models mentioned (viz. Rice, K, and homodyned K distributions), and then show the two parameters derived from the homodyned K distribution model and results obtained from fitting the model to experimental observations.

2. HOMODYNED K DISTRIBUTION MODEL

Ultrasound B-scan imaging involves receiving pulse echo signals reflected from a scattering medium. The received signal (actually the acoustic pressure received at the transducer) is a sum of signals (acoustic pressure) reflected by a large number of scattering points located within a resolution cell defined as the volume of medium that contributes towards the signal at a particular instant of time. These scatterers are randomly located and backscatter a random amount of energy, so the net signal has a statistical nature. We will first summarize the Rayleigh distribution, the Rice distribution and the K distribution used to model such an echo signal, and will combine them to obtain the homodyned K distribution model [7].

2.1. Rayleigh distribution model

The echo signal from scattering media can be modeled as a sum of backscatter signals from a number of scattering points in the media [1,6,12]. This sum is a complex sum due to random phase variations from random locations of the scatterers and random amplitude variations from random backscatter coefficients of each individual scatterer. So the received radio frequency (rf) signal can be written as [1]

$$z(t) = x(t)\cos(\omega_0 t) + y(t)\sin(\omega_0 t)\ , \tag{1}$$

where ω_0 is the central frequency of the ultrasound pulse, and, $x(t)$ and $y(t)$ are real and imaginary parts of the complex sum of the echo signal from each scatterer. Assuming that the phase of each backscattered signal is uniformly distributed and the number of scatterers is large with no fluctuations in the number of scatterers (using the central limit theorem), $x(t)$ and $y(t)$ are zero mean independent Gaussians. Therefore, the joint distribution function is given by

$$p_{xy}(x,y) = \frac{1}{2\pi\sigma^2}\exp\left(-\frac{x^2(t)+y^2(t)}{2\sigma^2}\right)\ , \tag{2}$$

where σ^2 is the variance of the Gaussian distributed $x(t)$ and $y(t)$.

The amplitude of the echo signal is given by

$$A(t) = \sqrt{x^2(t)+y^2(t)}\ . \tag{3}$$

Using rectilinear to polar coordinate transformation, the distribution function for echo

envelope amplitude, $A(t)$, can be shown to be the Rayleigh distribution function [13, pp. 44-50],

$$p_A(A) = \frac{A}{\sigma^2} e^{-A^2/2\sigma^2} . \tag{4}$$

This distribution function has been used to model the ultrasound echo signal [1–4]. But the problem with this model is that it assumes a large number of uniformly spatially distributed scatterers and a nonvarying scatterer density throughout the medium. Unless these strict conditions are satisfied, this model is not very useful.

2.2. Rice distribution model

The Rice distribution model is an extension of the Rayleigh distribution model that adds a "coherent" signal (homodyning signal, which is a deterministic signal) to the random backscatter signal of Eq. (1). The derivation of the Rice distribution model was given by S. O. Rice [14] in which he derived a model for shot noise currents. That derivation can be applied to model the echo signals received from a scattering medium as [1]

$$z(t) = x(t)\cos(\omega_0 t) + y(t)\sin(\omega_0 t) + s(t)\cos(\omega_0 t + \phi(t)) , \tag{5}$$

where the first two terms on the right hand side are same as the ones in Eq. (1) and the third term describes the homodyning signal from "structure" or periodic scatterers. The first two terms in Eq. (5) describe the quadrature components of the signal from randomly distributed scatterers and contribute to the so called "diffuse" scattered signal. The third term in the equation describes the "coherent" component of the signal. In this "coherent" component, $s(t)$ is the nonrandom amplitude of the coherent (or homodyning) signal and $\phi(t)$ is its (nonrandom) phase. The distribution function for $z(t)$ can be written as

$$p_{xy}(x, y) = \frac{1}{2\pi\sigma^2} \exp\left\{ -\frac{[x(t) + s(t)]^2 + y^2(t)}{2\sigma^2} \right\} . \tag{6}$$

The envelope of this rf signal is given by

$$A(t) = \sqrt{[x(t) + s(t)]^2 + y^2(t)} . \tag{7}$$

The probability distribution function for the above echo envelope signal is given by [13, pp. 45-50],

$$p_A(A) = \frac{A}{\sigma^2} e^{-[A^2+s^2]/2\sigma^2} I_0\left(\frac{As}{\sigma^2}\right) , \tag{8}$$

where $I_0(x)$ is the modified Bessel function of first kind and σ^2 is the variance of the two quadrature components.

This distribution is Rayleigh for $s = 0$ (i.e., no coherent component) and becomes Gaussian for large value of s ($s \to \infty$, i.e., with a large coherent component and small diffuse component).

From the Rice distribution model, the derived autocorrelation function and the spectrum have been used to analyze the echo signal to obtain tissue characterizing parameters [2–4].

2.3. K distribution model

While the Rice distribution models the unresolved structure (periodicity in scatterers) well, it fails to account for the case of media with clustering (nonuniformity in spatial distribution) in scatterers or with smaller effective number of scatterers. The K distribution, which is a generalization of the Rayleigh distribution with clustering in spatial distribution

of scatterers, has been used earlier to model this situation [8,9]. Using a random walk to model scattering, Jakeman has used the K distribution for amplitude statistics of laser speckle [7]. Using the negative binomial distribution (this distribution models variable mean Poisson processes [7]) to model the distribution of scatterer density (therefore assuming that scatterer density is also a random variable), the amplitude density function was derived to be [7]

$$p_A(A) = \frac{2b}{\Gamma(\mu)}\left(\frac{bA}{2}\right)^{\mu} K_{\mu-1}(bA)\,, \tag{9}$$

where μ is a parameter of the negative binomial distribution used to model the scatterer density distribution (a measure of clustering in scatterers or effective number of scatterers [9, 15]). In this equation, $b = 2(\frac{\mu}{<A^2>})^{1/2}$ (where $<>$ is the expectation operator) and $K_{\mu-1}(x)$ is the modified Bessel function of second kind. Using the notations of the Rice distribution model, one can use $< A^2 >= 2\sigma^2$. For the case of large μ (i.e., $\mu \to \infty$), the K distribution converges to a Rayleigh distribution.

The K distribution has been used to model microwave sea echoes [15], laser speckle in atmospheric transmission [7], and ultrasound echo speckle [9,10,16].

From the above two analyses, we see that the Rice distribution is a generalization of the Rayleigh distribution and allows for structural (or periodic) components in the echo signal. The K distribution is a generalization that allows for clustering of scatterers (or reduced effective number of scatterers) in the medium. This suggests that a combination of the above two generalizations could be a better way to model the echo signal.

2.4. Homodyned K distribution model

Jakeman has shown that a combination of features from the Rician generalization and the K distribution generalization, the homodyned K distribution, is better suited to model speckle in cases of scattering from turbulent scattering media [7]. This model combines the homodyning effects of the Rice distribution with small scatterer properties of the K-distribution to give a better model for typical scattering in tissues. The homodyning term gives the expression for the probability distribution function of the amplitude of the echo envelope [11];

$$p_A(A) = A\int_{u=0}^{\infty} u\frac{J_0(us)J_0(uA)}{(1+\frac{u^2\sigma^2}{2\mu})^{\mu}}du\,, \tag{10}$$

which evaluates to

$$p_A(A) = \frac{1}{\Gamma(\mu)}\left(\frac{A}{s}\right)^{\frac{1}{2}}\sqrt{\frac{2\mu}{\pi\sigma^2}}\sum_{m=0}^{\infty}\left\{(-1)^m\frac{\Gamma(m+\frac{1}{2}}{m!\Gamma(\frac{1}{2}-m}\left(\frac{\sigma^2}{sA\mu}\right)^m\right.$$
$$\left.\left(\frac{\mu}{2\sigma^2}\right)^{\frac{\mu+m-1/2}{2}}|s-A|^{\mu+m-1/2}K_{\mu+m-1/2}\left(\sqrt{\frac{2\mu}{\sigma^2}}|s-A|\right)\right\}\,, \tag{11}$$

where the parameters are the same as in the previous two models: the Rice and the K distributions.

Even though the expression for the distribution function involves an infinite series, the equations for the even moments of this distribution, (as in case of the Rice and K

distributions) have closed form expressions [11]:

$$< A^{2r} >= \left(\frac{2\sigma^2}{\mu}\right)^r r! \frac{\Gamma(r+1)}{\Gamma(\mu)} \sum_{p=0}^{r} \frac{\Gamma(\mu+r-p)}{\Gamma(p+1)p!(r-p)!} \left(\frac{s^2\mu}{2\sigma^2}\right)^p . \tag{12}$$

Using the above equation for even moments of the distribution, the first three moments can be expressed as

$$< A^2 > = s^2 + 2\sigma^2 , \tag{13}$$

$$< A^4 > = 8\left(1 + \frac{1}{\mu}\right)\sigma^4 + 8\sigma^2 s^2 + s^4 , \tag{14}$$

and

$$< A^6 > = 48\left(1 + \frac{3}{\mu} + \frac{2}{\mu^2}\right)\sigma^6 + 72\left(1 + \frac{1}{\mu}\right)\sigma^4 s^2 + 18\sigma^2 s^4 + s^6 . \tag{15}$$

The above three equations can be used to estimate the three parameters: s^2 (the coherent signal energy), σ^2 (the diffuse signal energy) and μ (the scatterer clustering parameter) from the moments of the distribution.

Because μ always appears as $\frac{1}{\mu}$ in the above equations for moments, we will solve for a derived parameter, $\beta = \frac{1}{\mu}$. The value of β will be small for no clustering or equivalently for large numbers of independent scatterers in the resolution cell and will be large otherwise. To give an estimate of the extent of "structure" in the resolution cell signal or the periodicity in the scatterer locations, we will use a derived parameter, k, which will be defined as the ratio of coherent signal to diffuse signal ($k = \frac{s}{\sigma}$). As k is a ratio, it gives a signal amplitude independent measure of the extent of structure (resolved or unresolved periodic backscattered energy). The above two parameters should provide characterizing indices for a given medium.

2.5. Parameter estimation

The three equations, Eqs. (13)-(15), can be used to solve for the three parameters: s^2, σ^2, and β. As the three equations are nonlinear, nonlinear (iterative type) methods will have to be employed for solving them. The method employed here was the trust region method in conjunction with Newton's method. Freely distributed FORTRAN code, NNES (Nonmonotonic Nonlinear Equation Solver) [17] was used to develop the equation solver that solved for the three parameters: s^2, σ^2, and $\beta = \frac{1}{\mu}$.

3. SIMULATIONS

Simulated echo signals were generated with varying scatterer densities, backscatter coefficients, and clustering to test the parameter estimation using the moments equations: Eqns. (13)-(15). To simulate a "coherent" signal, periodically located scatterers were used; the "diffuse" component was simulated using randomly located scatterers with randomly distributed backscatter coefficients. The simulations were done in 2D because 3D simulations involve just an addition of one more dimension which does not make any difference to the statistical model. All the scatterers are assumed to be point scatterers. A 3.0 MHz central frequency was assumed for the simulated signal, with 1.6 μs pulse length. The simulated beam was Gaussian shaded along the aperture and in the time domain. The sampling frequency along depth was 10 MHz. Simulated A-lines in the plane of scanning were 2 mm apart. The resolution cell size was estimated using the "correlation length" (defined as

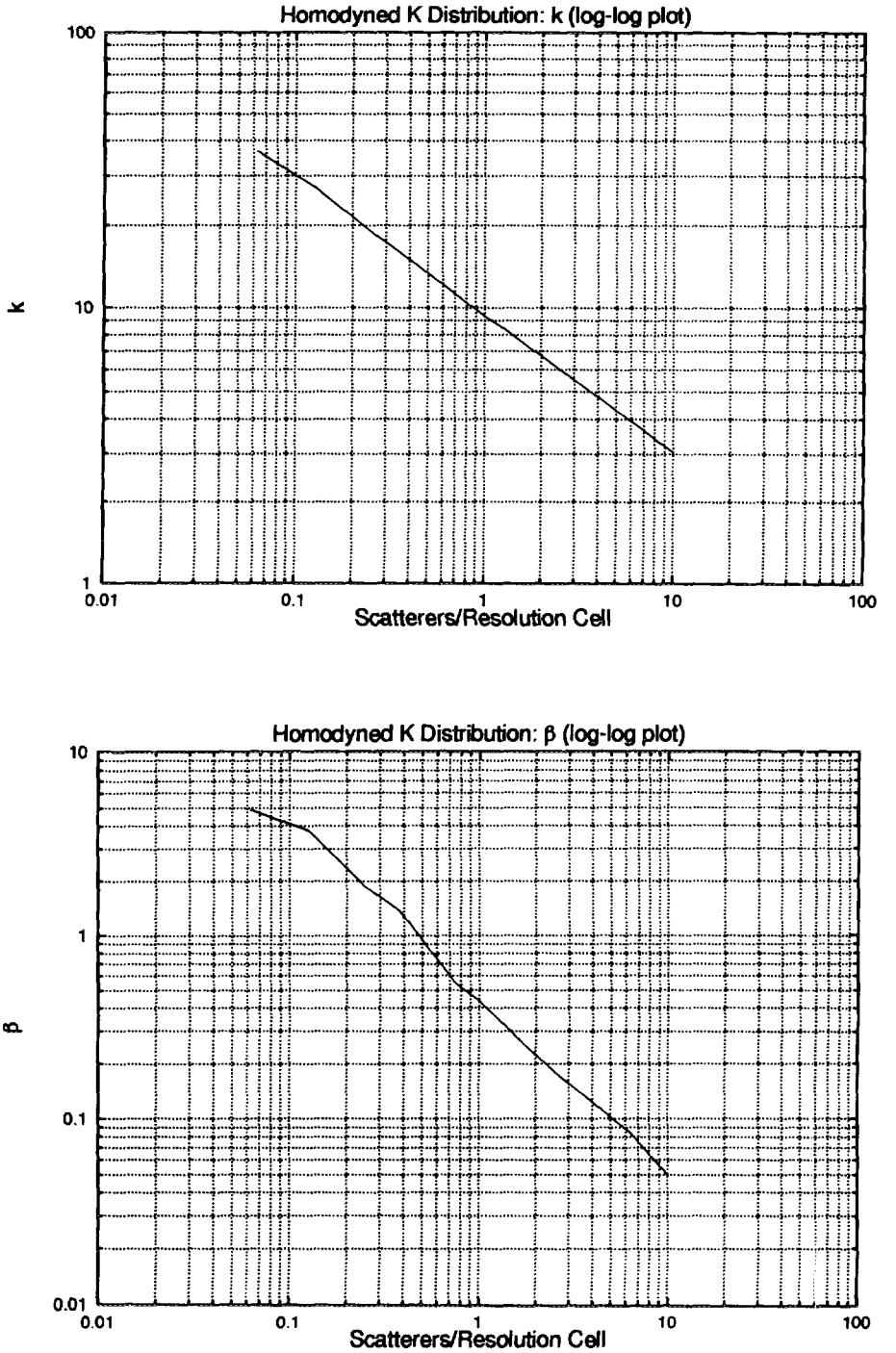

Fig. 1 Estimates of k and β for various scatterer densities calculated from simulation data using the homodyned K-distribution model: The plots are log-log plots. The parameters were obtained from moments estimates using 2048 envelope data points (64 A-lines of 32 envelope points).

the normalized integral of the autocorrelation function) method. The estimated resolution cell size was 0.53 mm^2. To study the effects of backscatter coefficient variations and the scatterer density variations, two types of simulations were done:

1. Simulations to study the parameter variations with change in scatterer density, and,
2. Simulations to study variation in parameters with change in "diffuse"; backscatter signal level and "clustering".

For the first set of simulations, the scatterer density was varied from 0.1 scatterers/resolution cell to 35 scatterers/resolution cell. The second set of simulations were done at 10 scatterers/resolution cell, with a "coherent" component around 24 times the "diffuse" component at 0.17 scatterers per resolution cell. Both the simulations used 2048 sample points (64 A-lines of 32 points each) to estimate the sample moments. This scanned area corresponds to the volume of approximately 21.4 resolution cells. 128 independent sets were obtained for computing the statistics.

4. RESULTS: SIMULATIONS

Figure 1 shows the variation of parameters k and β as a function of the number of scatterers per resolution cell. The plots clearly show that the diffuse signal level increases with the number of scatterers (hence k decreases with increased scatterer density). The slope of the log-log plot (slope of approximately -0.5) indicates a square root dependence of diffuse signal level on number of scatterers per resolution cell. The squre root dependence is as expected for a finite sum of random phasors. The inverse of β, i.e., μ, increases linearly with scatterer density (the slope of log-log plot of β vs. number of scatterers per resolution cell is close to -1.0), which is expected because μ is proportional to the effective number of scatterers in the resolution cell.

In the second set of simulations, the parameters were estimated for different combinations of backscatter coefficients for the scatterers and for different clustering factors. The simulations were done at 10 scatterers per resolution cell. The clustering effect was simulated by clustering the randomly located scatterers around some randomly located cluster centers. The clustering parameter shown in the plots is not directly related to β but is just a measure of clustering. Figure 2 shows that k remains constant with change in clustering, as one would expect for point scatterers assumed in our simulations. Also, k decreases with increased backscatter coefficient because k is inversely related to the backscatter coefficient. Figure 3 shows that the parameter β remains constant with change in backscatter coefficient, but increases with clustering as expected. These plots show that k and β provide two parameters to characterize the echo signal from biological tissues or any such medium under echo ultrasound examination.

5. EXPERIMENTS WITH PHANTOMS

To test the simulations, a set of phantoms with various scatterer densities were scanned using a laboratory echo ultrasound system. This system consists of a water tank in which the sample to be imaged is placed at one end and the transducer is placed at the other end in a two axis motorized assembly, which allows for moving the transducer in horizontal plane perpendicular to the beam axis (Fig. 4). The two stepper motors are computer controlled to allow full position control. The stepper motors allow displacements in steps of 0.025 mm in the horizontal plane and 0.02 mm in the vertical plane. The stepper motor assembly is controlled by a CRDS Universe 68000 computer that also controls the triggering of the echo

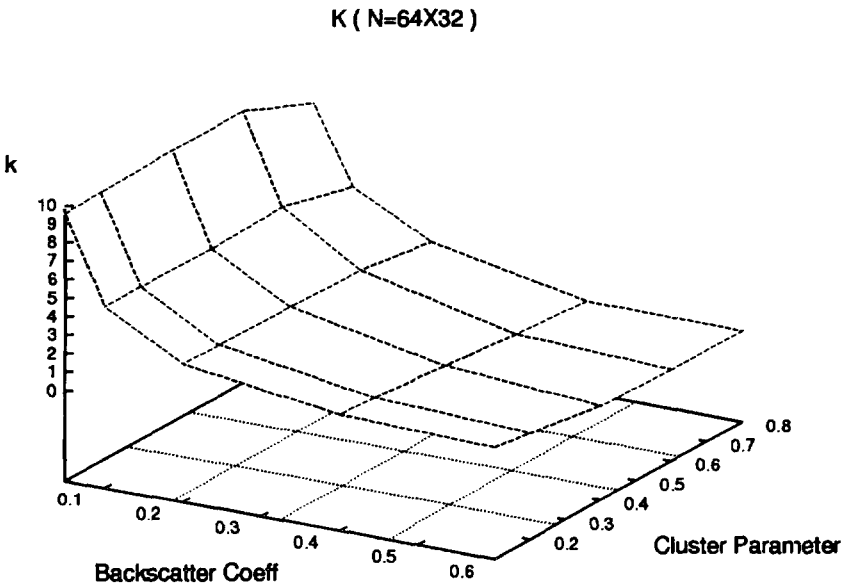

Fig. 2 Mean estimates of k clustering and backscatter level calculated from the homodyned K-distribution model. The parameters were obtained from moments estimated using 2048 envelope data points (64 A-lines of 32 envelope points).

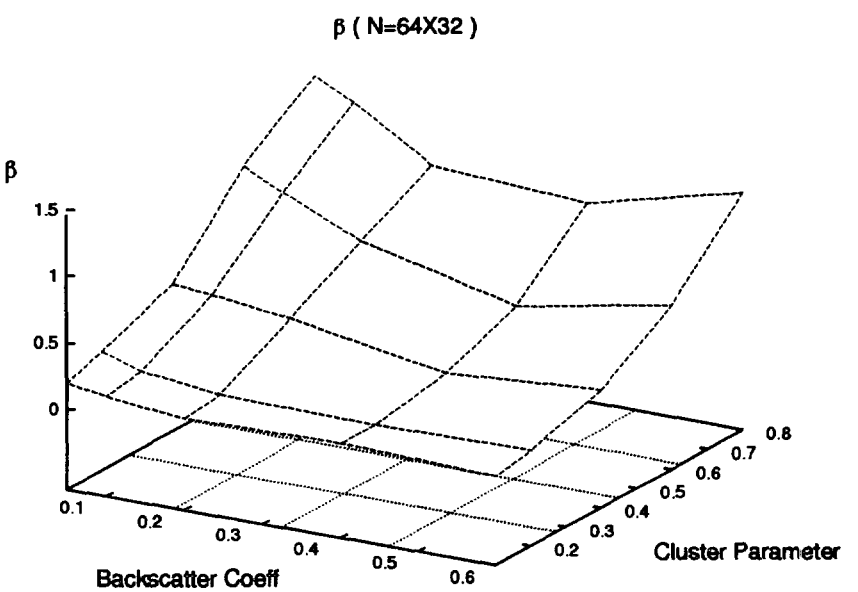

Fig. 3 Mean estimates of β versus backscatter coefficient and clustering factor of the scatterers calculated from the homodyned K distribution model. The parameters were obtained from moments estimated using 2048 envelope data points (64 A-lines of 32 envelope points).

system and receives the digitized data. The data were subsequently transferred to a Sun workstation for signal analysis. A set of six commercially made phantoms (ATS laboratories, Bridgeport, CT) made of silicon rubber based material in which fine glass beads, of average diameter 68 μm, are mixed for scattering, were used for the experiment. These phantoms had scatterer densities of 8.55, 17.05, 42.83, 67.89, 151.98, and 428.35 scatterers/mm^3. The phantoms were scanned with three transducers having central frequencies of 3.5, 5.0, and 7.5 MHz. A three-dimensional volume was scanned to obtain a large set of data points. The data sampling rate for depth (x-axis in figure 4, the axis of the transducer, or the A-line axis) was 40 MHz. The y-axis sampling width was 0.4 mm and the z-axis sampling width was 1.0 mm. Each A-line was digitized with an 8-bit A/D converter at 40 MHz after amplifcation with a low noise amplifier. These data were subsequently subsampled to 10 MHz after envelope detection. The echo signal was sampled in the focal region of the transducers. The resolution cell sizes were measured with the "correlation length" method as the integral of the normalized autocorrelation function of the envelope in 3D. The estimated resolution cell sizes at the three frequencies were 0.21 mm^3, 0.07 mm^3, and 0.02 mm^3 at 3.5, 5.0, and 7.5 MHz respectively. The resolution cell size was estimated from the volume enclosed by the envelope signal contour at -20 dB level from a point scatterer. Cell size was determined the same way for the simulations. As in the case of the simulation study, the statistics were estimated using 2048 data points. These data were obtained for two combinations: 64 A-lines with 32 points along each A-line and 128 A-lines with 16

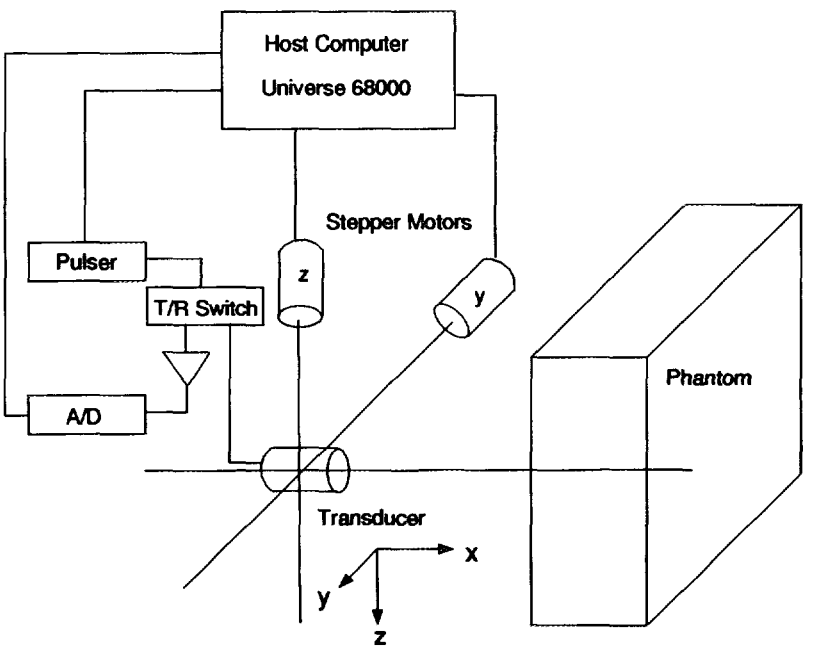

Fig. 4 Phantom scanning geometry: The phantom to be scanned is placed in a water tank opposite the scanning transducer whose position is controlled by a computerized two axis motor assembly. The received rf data are digitized and stored on the controlling computer.

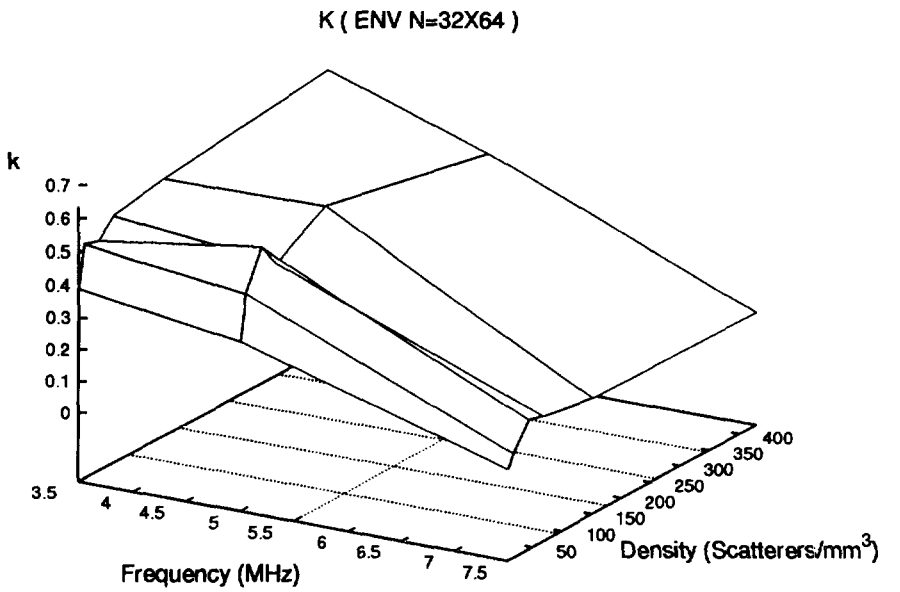

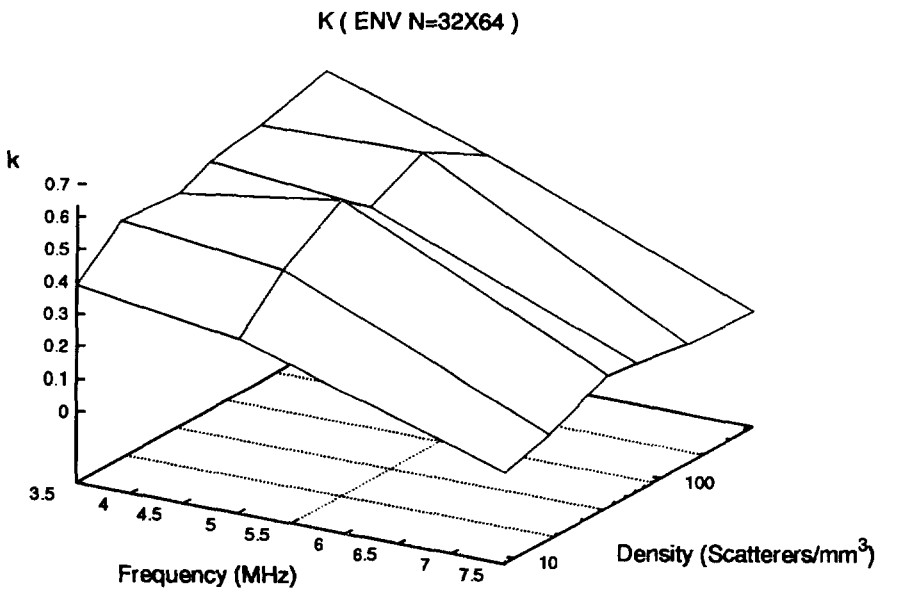

Fig. 5 Mean estimates of k versus scatterer density and signal frequency. Each estimate is calculated from 64 A-lines of 32 envelope samples using the homodyned K distribution model. Top plot is with linear scale and bottom is with logarithmic scale for scatterer density.

points along each A-line. This corresponds to areas of 25.6 mm width by 1.2 mm depth and 12.8 mm width by 2.4 mm depth respectively. The results are reported for variations with the scatterer density (scatterers/mm^3) and variations with scatterers per resolution cell.

In our statistical modeling, we assumed that there is no significant attenuation in the A-lines along the depth as this would alter the statistics of the echo signal distribution. To minimize the effects of attenuation, the number of points taken along the depth were quite small (16 or 32 points corresponding to a depth of 1.2 mm and 2.4 mm, respectively). To study the effects of attenuation compensation, statistics and parameters were also evaluated for attenuation compensated (TGC) signals. The attenuation was estimated by simple least squares fit of an exponential decay to the envelope signal.

6. RESULTS: PHANTOMS

The experiment set-up employed some phantoms with low and some with high scatterer densities. In the high density phantoms, deviation from perfect randomness in spatial distribution was expected because at such high densities the finite size of individual scatterers would impose restrictions on the random placement of these scatterers. As expected, the SNR (signal to noise ratios, computed as the mean divided by the standard deviation) for amplitude and intensities were above 1.91 and 1.0 respectively, which are the upper limits for the K distribution, suggesting a "coherent" component to the echo envelope signal. Figures 5-8 show 3D plots of k and β versus scatterer density (or number of scatterers per resolution cell). These plots are logarithmically scaled because the density variation is large. The k value for these phantoms is very small (less than 1) which shows that the "coherent" component is not very large. However, the parameter shows a decrease with an increase in frequency that is the result of a decrease in the effective number of scatterers per resolution cell. This correlates with the fact that with large increases in effective scatterer densities, there is a possibility of some order in the spatial structure of scatterer distribution as well as the possibility that effective scatterer size becomes large, giving rise to specular reflection which should give rise to a "coherent" component in the echo signal. Similarly k increases with the scatterer density, which could be explained in terms of decrease in randomness of the distribution or rise in specular scattering contributing to some coherent component. The β value shows a decrease with scatterer density as expected. The decrease in β is more obvious for 7.5 MHz scanning because the effective scatterer density is very low at that frequency. The β value should slightly increase in value for large scatterer density, which again could be explained as due to clustering in scatterers at large densities.

The demonstrated variation in these parameters with frequency is as expected. With increase in frequency, the resolution cell size drops, which reduces the effective number of scatterers per resolution cell. This results in an increase in β, which is what we obtain. Even though the variations in k are somewhat complex because k depends both on the effective number of scatterers as well as the backscatter coefficient that is a function of frequency, in our experiment, we see that k decreases with increased frequency and increases with scatterer density. This could be explained by a reduction in orderliness in the spatial distribution or a rise in specular scattering as the decrease in the resolution cell size results in smaller scatterer numbers per resolution cell.

To see the effect of attenuation compensation on this statistical scattering model, exponential time gain compensation (TGC) was used on these envelope A-lines. The attenuation coefficient was estimated by fitting an exponential decay to the A-lines. Parameter estimates for these time gain compensated signals are shown in figures 9-12. Time gain compensation reduces the variance of the estimates. This is expected because the effect of attenuation on the probability density function of the envelope amplitude is somewhat compensated for. The variation in β is much sharper as seen in these figures. The drop in β with increase

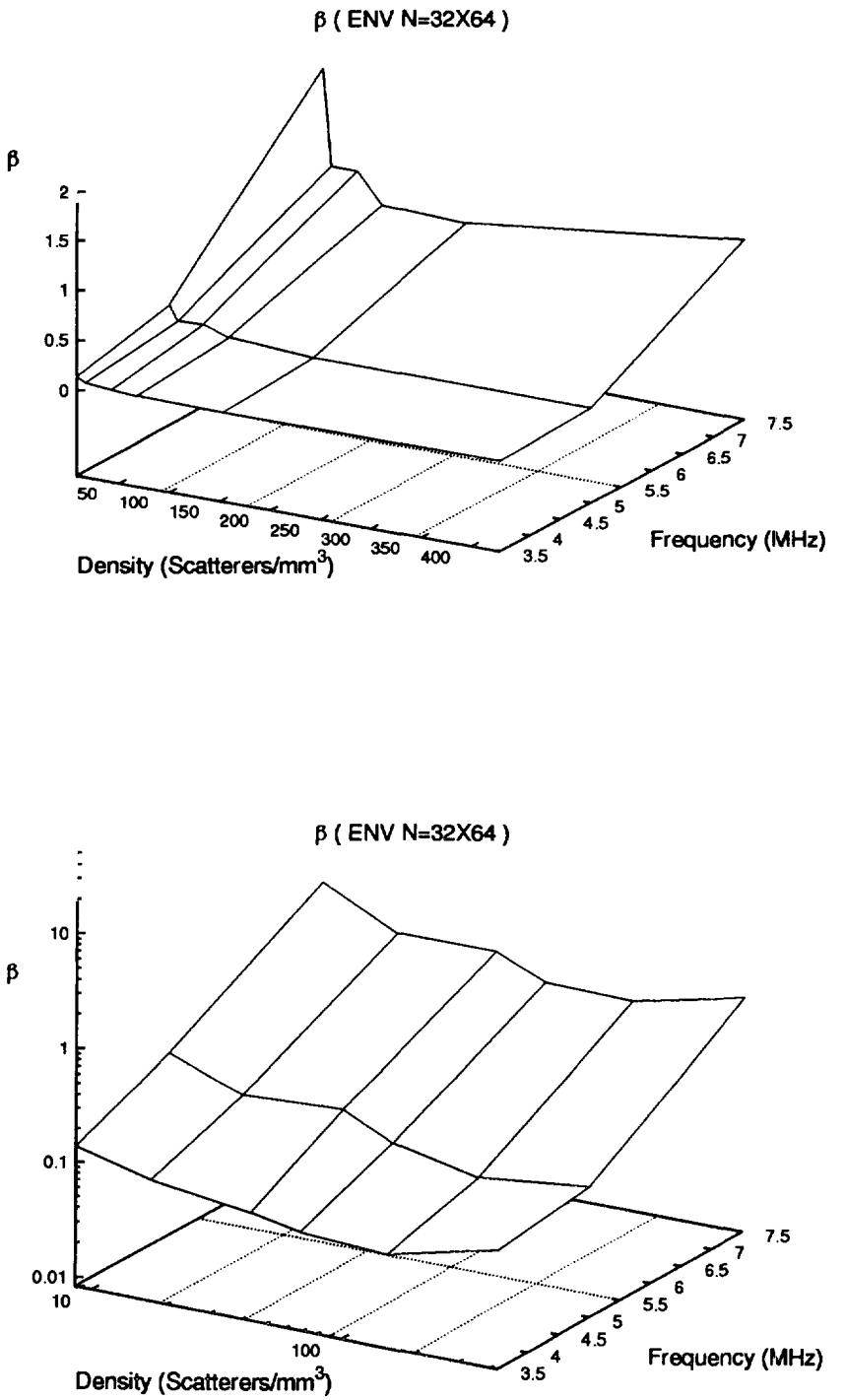

Fig. 6 Mean estimates of β versus scatterer density and signal frequency. Each estimate is calculated from 64 A-lines of 32 envelope samples using the homodyned K distribution model. Top plot is with linear scale and bottom is with logarithmic scale for scatterer density.

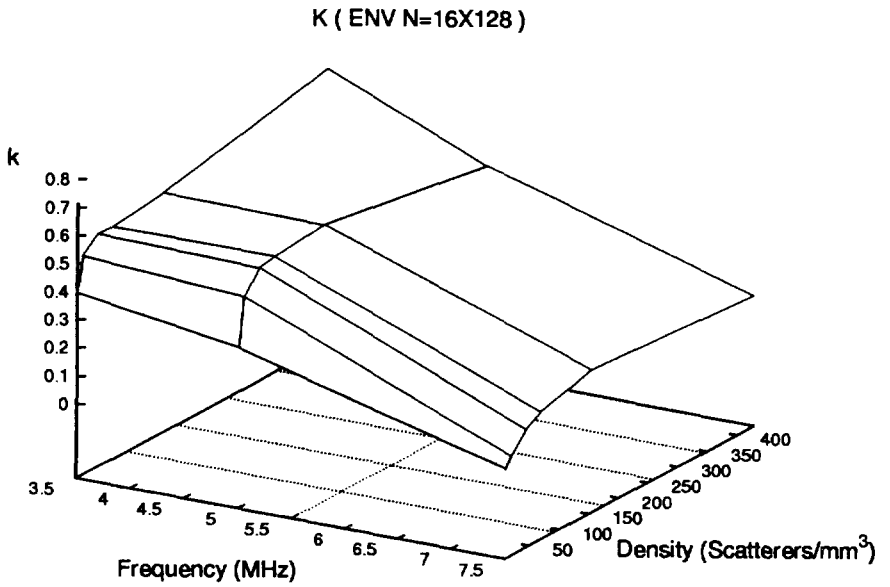

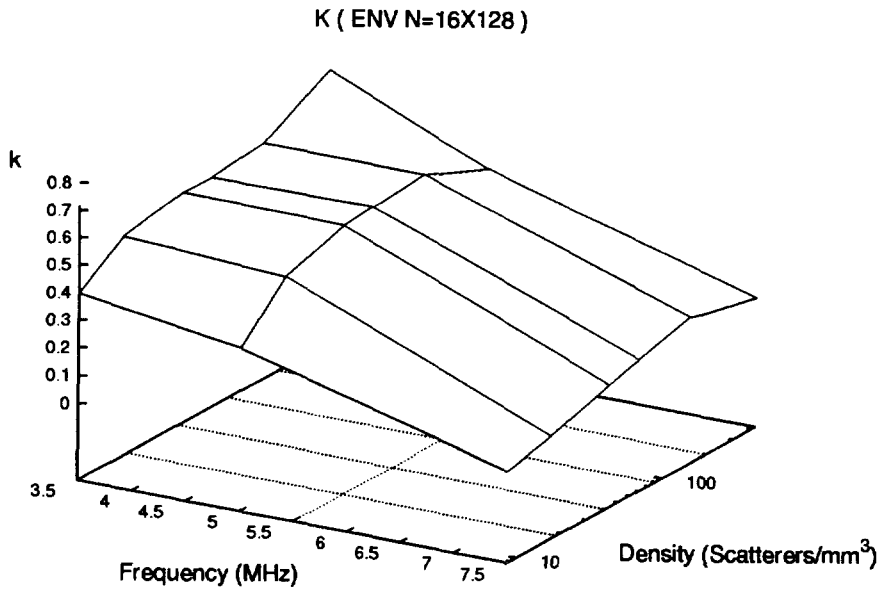

Fig. 7 Mean estimates of k versus scatterer density and signal frequency. Each estimate is calculated from 128 A-lines of 16 envelope samples using the homodyned K distribution model. Top plot is with linear scale and bottom is with logarithmic scale for scatterer density.

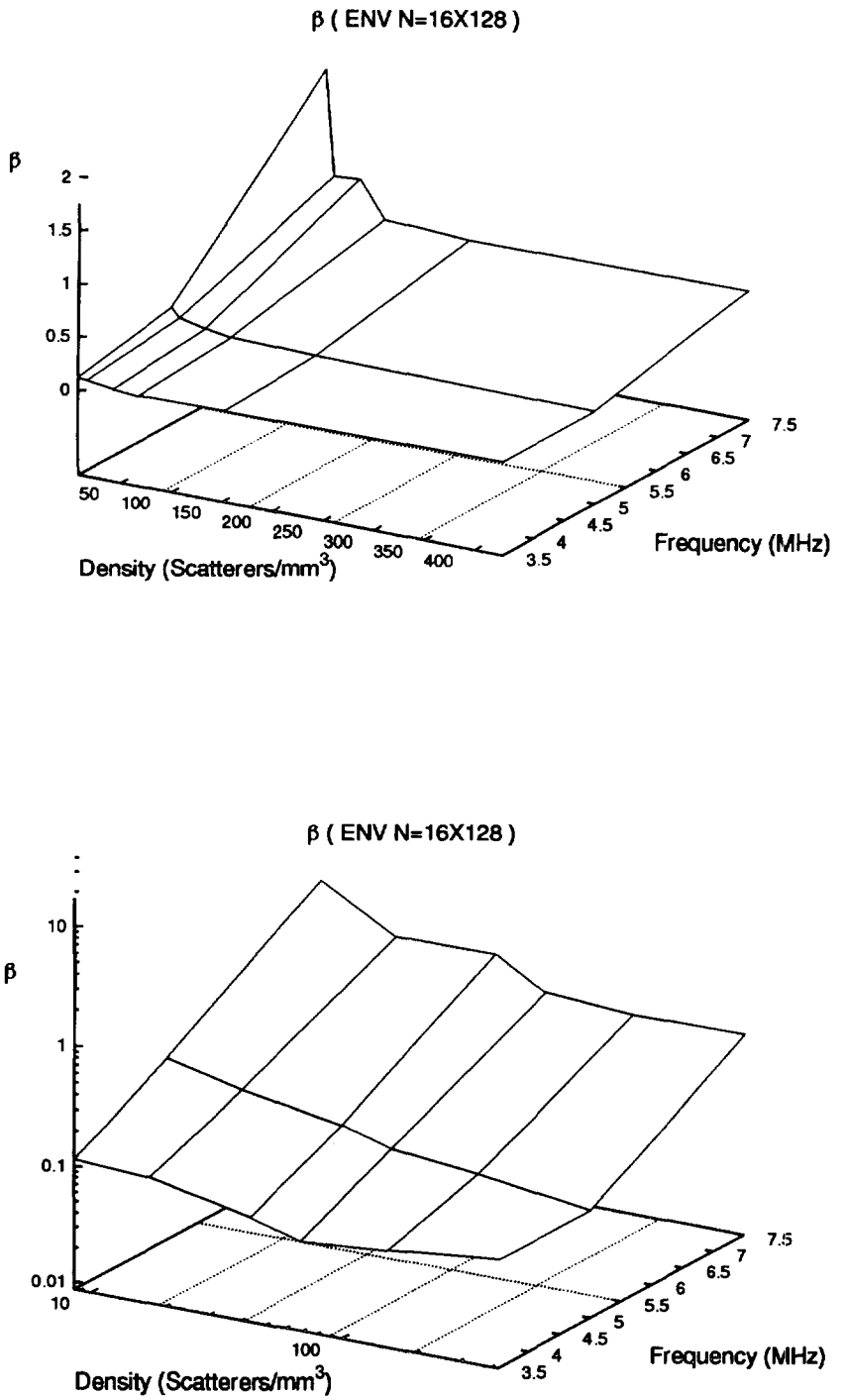

Fig. 8 Mean estimates of β versus scatterer density and signal frequency. Each estimate is calculated from 128 A-lines of 16 envelope samples using the homodyned K distribution model. Top plot is with linear scale and bottom is with logarithmic scale for scatterer density.

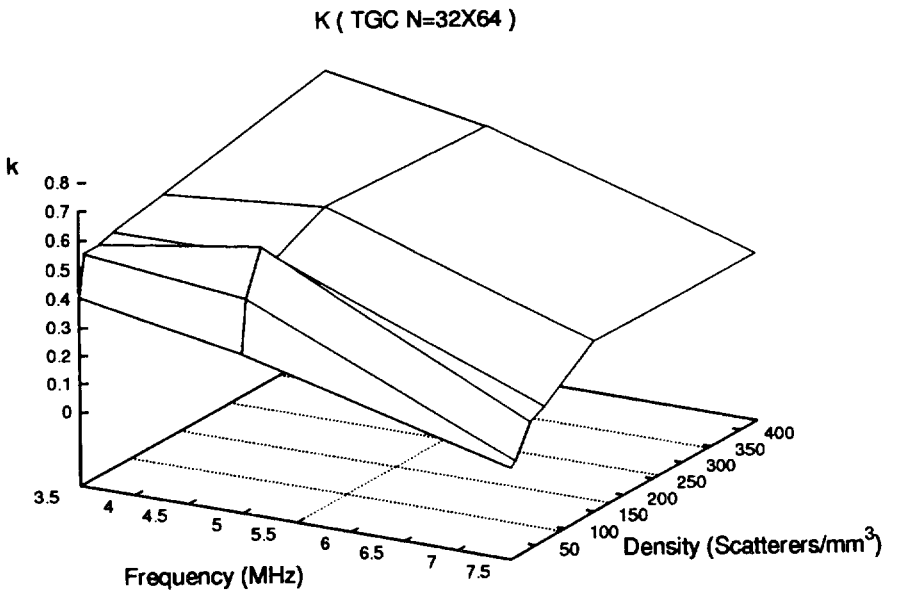

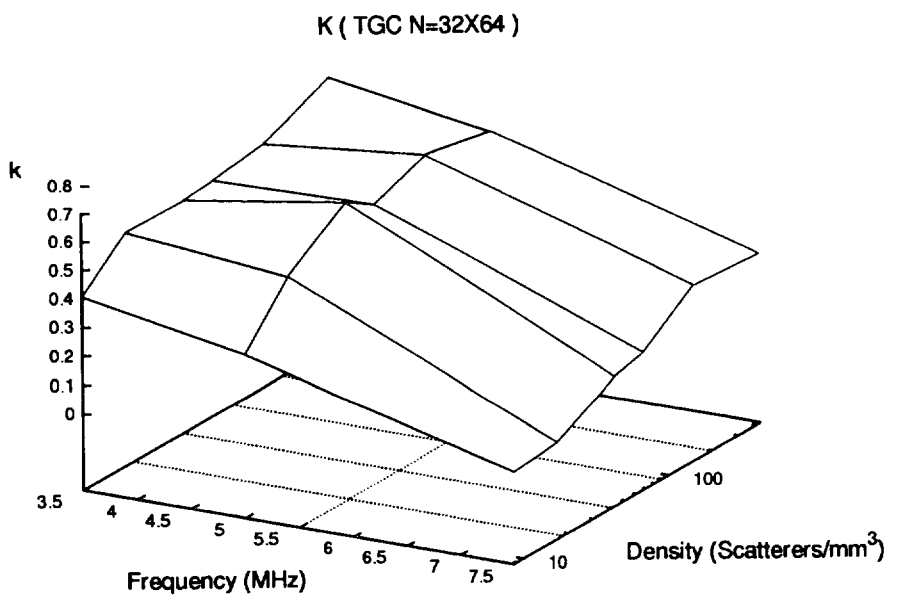

Fig. 9 Mean estimates of k versus scatterer density and signal frequency for time gain compensated (TGC) data. Each estimate is calculated from 64 A-lines of 32 TGC envelope samples using the homodyned K distribution model. Top plot is with linear scale and bottom with logarithmic scale for scatterer density.

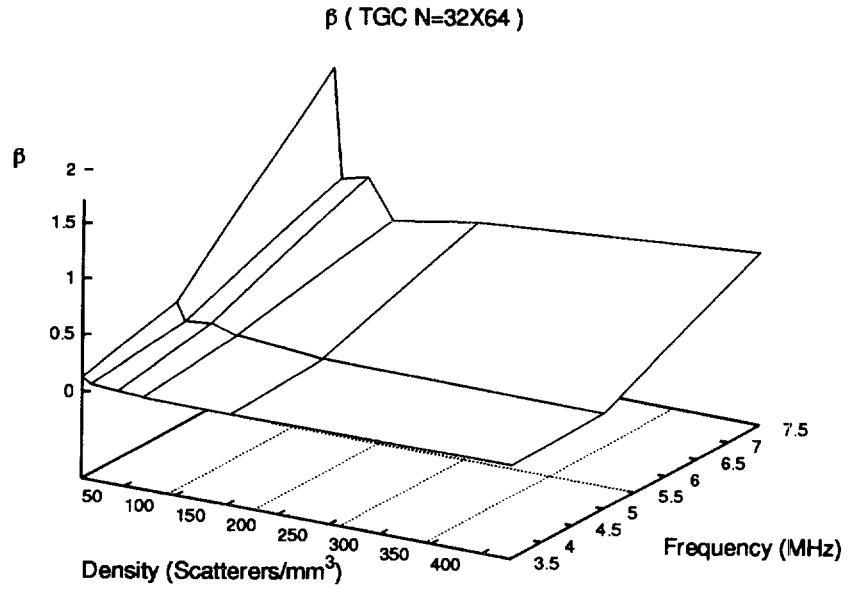

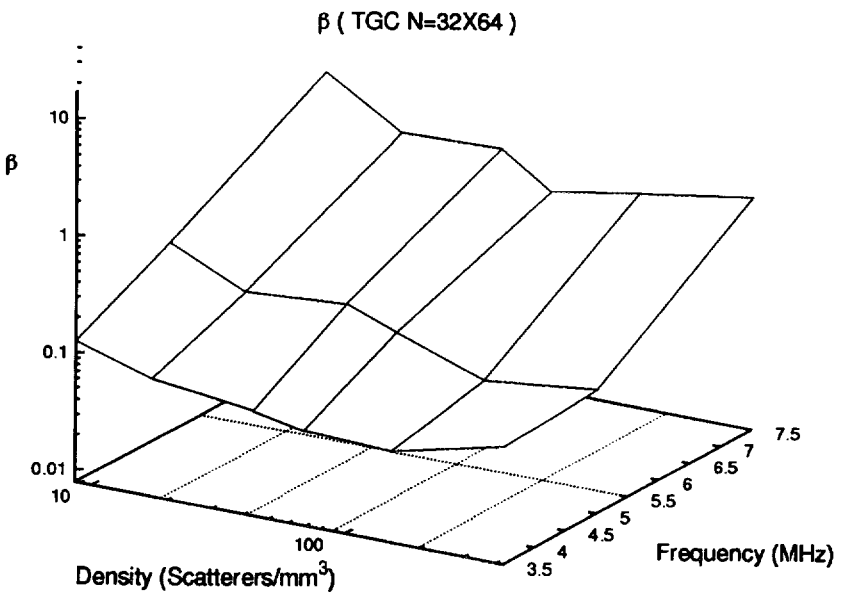

Fig. 10 Mean estimates of β versus scatterer density and signal frequency for time gain compensated (TGC) data. Each estimate is calculated from 64 A-lines of 32 TGC envelope samples using the homodyned K distribution model.

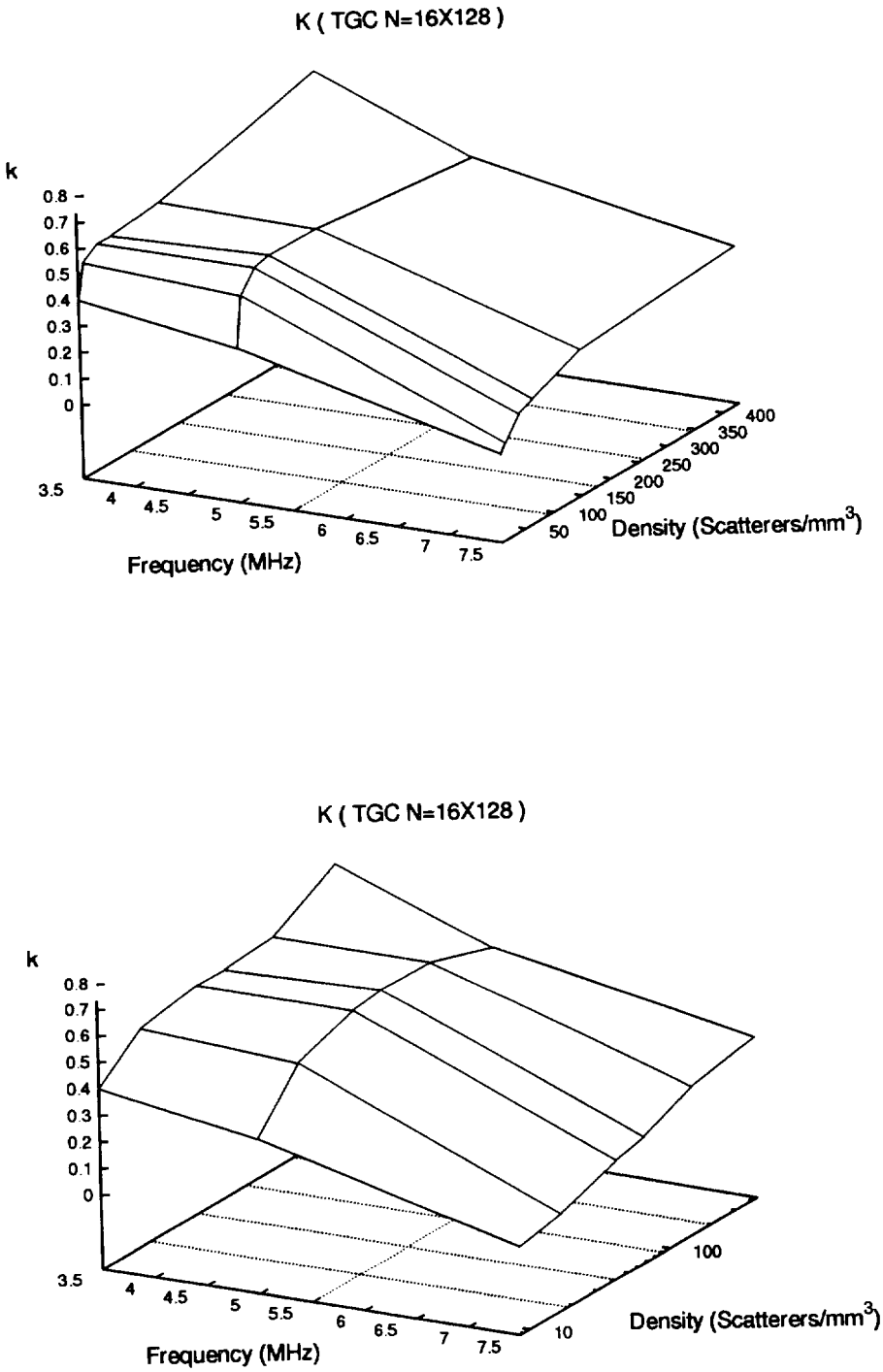

Fig. 11 Mean estimates of k versus scatterer density and signal frequency for time gain compensated (TGC) data. Each estimate is calculated from 128 A-lines of 16 TGC envelope samples using the homodyned K distribution model. Top plot is with linear scale and bottom is with logarithmic scale for scatterer density.

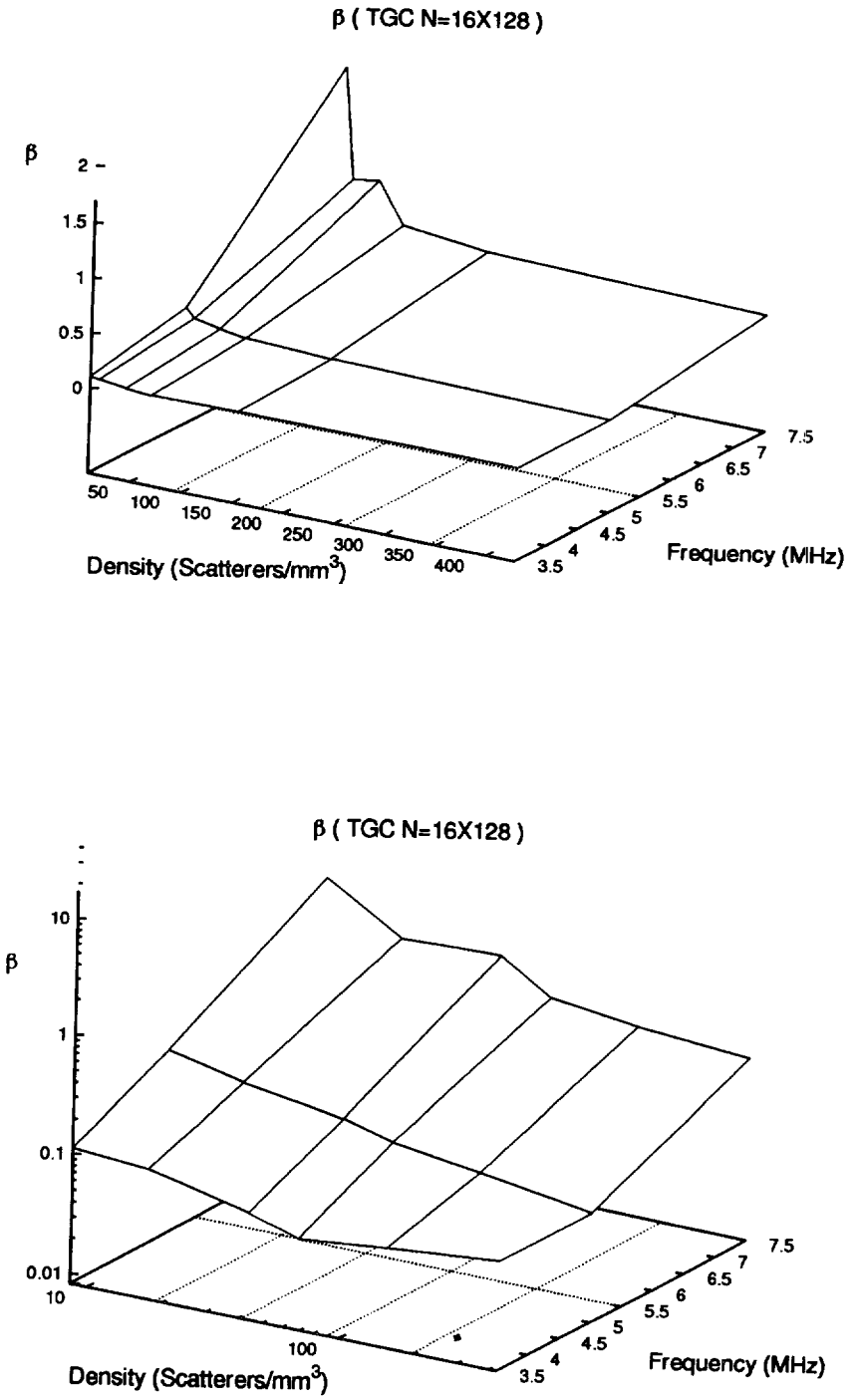

Fig. 12 Mean estimates of β versus scatterer density and signal frequency for time gain compensated (TGC) data. Each estimate is calculated from 128 A-lines of 16 TGC envelope samples using the homodyned K-distribution model. Top plot is with linear scale and bottom is with logarithmic scale for scatterer density.

in scatterers per resolution cell at 7.5 MHz scanning is significant, as expected. Also, the attenuation effects are stronger for the data sample in which 64 A-lines of 32 points along depth were taken as compared to samples in which 128 A-lines of 16 points along depth were taken. We would expect this because longer A-lines are more affected by attenuation.

Results from the phantom study show close agreement with the simulation results. The experimental results for the parameter k show that the parameter increases with decrease in frequency, which is expected if a decrease in frequency implies an increase the number of scatterers per resolution cell and the resultant orderliness in spatial distribution. But this parameter also depends on the variation of the backscatter coefficient with frequency and hence this complex variation could not be predicted with simulations. However, the variations in the parameter β can be compared because it is strongly dependent on the effective scatterer density. At frequencies of 3.5 and 5.0 MHz, the scatterer densities are just too high to show variations in β because β is fairly low. However, at 7.5 MHz, the effective scatterer density per resolution cell falls quite low, allowing good comparison with simulation estimates. From figures 13-16, we can see that simulation estimates show good correlation with estimates from the phantom given similar scattering densities. For the uncompensated signals, the estimated β is slightly larger than the simulation estimate, which could be due to higher attenuation effects at large scatterer densities. We see that when the attenuation is compensated for, the estimates of β are quite close to simulation estimates.

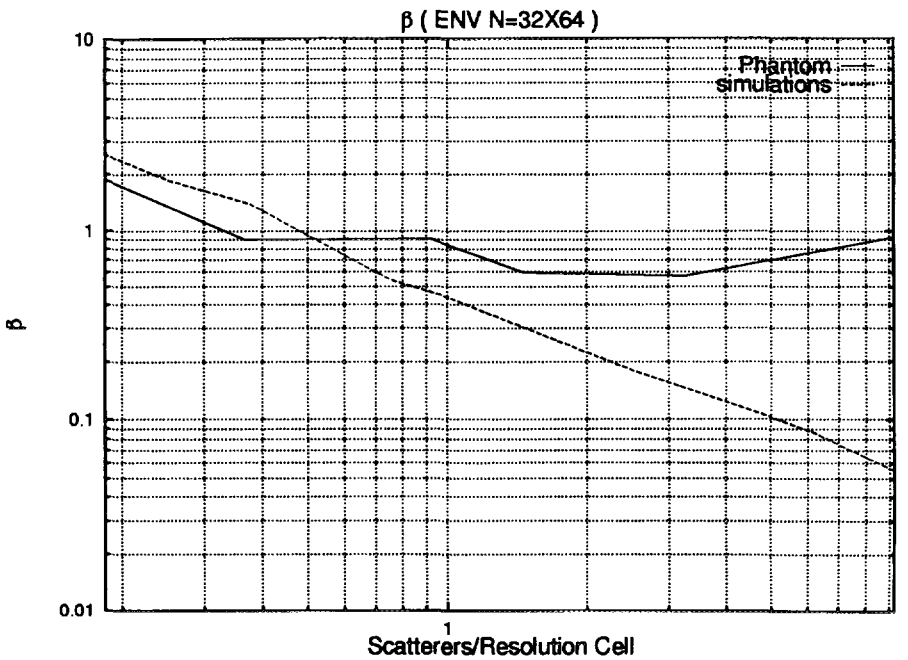

Fig. 13 Comparison of β estimated from experimental phantoms and simulation studies for 32X64 sample size.

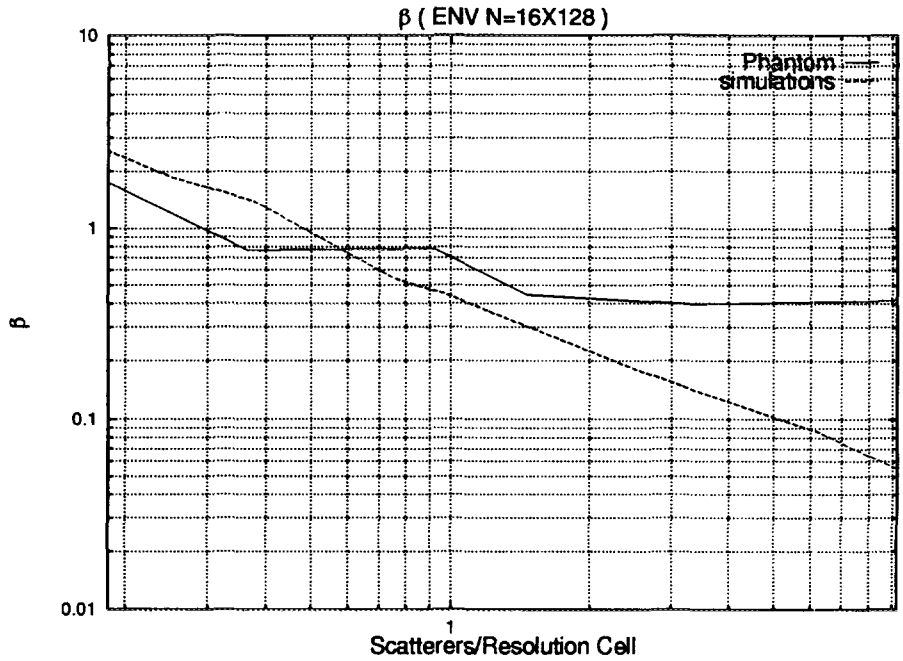

Fig. 14 Comparison of β estimated from phantoms and simulation studies for 16X128 sample size.

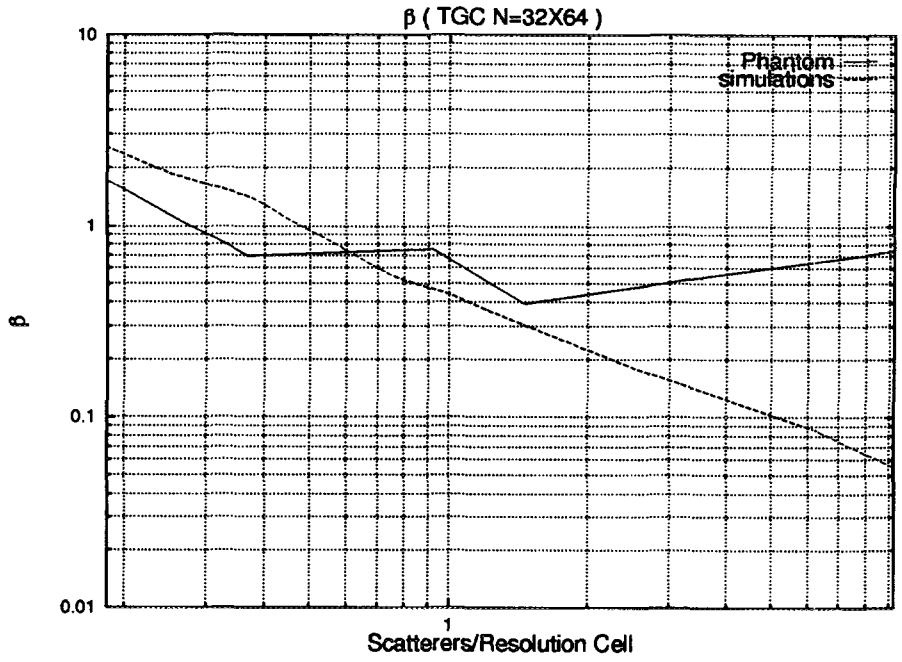

Fig. 15 Comparison of β estimated from experimental TGC phantom data and simulation studies for 32X64 sample size.

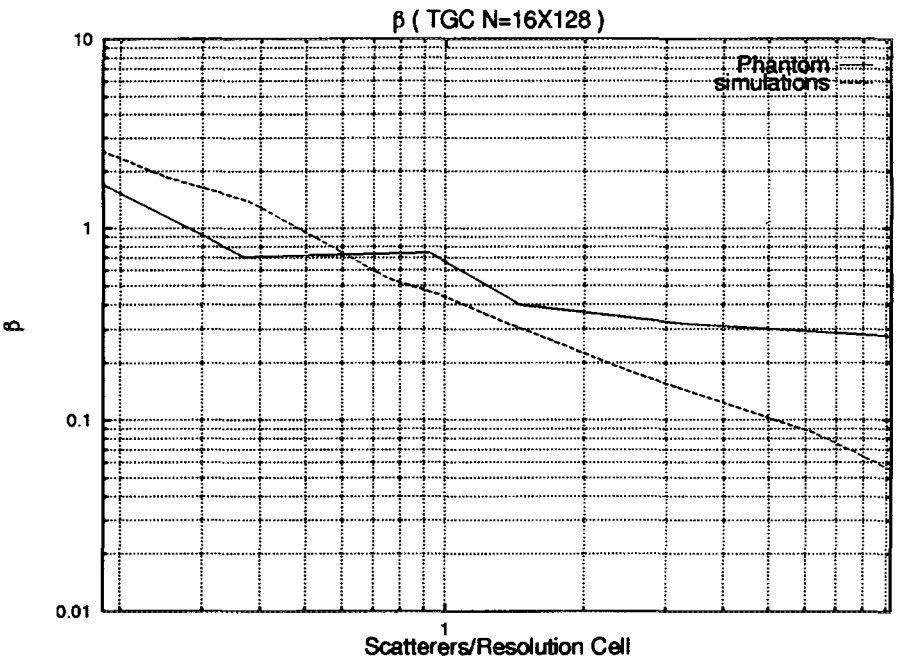

Fig. 16 Comparison β estimated from TGC phantom data and simulation studies for 16X128 sample size.

7. CONCLUSIONS

The results from computer simulations and experimental phantoms show that the parameters k and β calculated from the homodyned K distribution model give two independent measurements on the statistics of the echo signal: β gives information on the extent of clustering (nonuniformity in spatial distribution) of scatterers or effective number of scatterers per resolution cell, and k gives information on the backscatter coefficient and the structural (or periodically located scatterers) component of the scatterers. The results from the phantom experiments demonstrate the variation of β with change in scatterer density. The variation of k also shows predicted trends with the possibility of orderliness in spatial distribution at high scatterer densities.

These results show that this homodyned K distribution model should be useful for tissue characterization because the computed parameters reflect on the properties of the random scatterers as well as the structural scatterers. The use of this distribution allows modeling data with small SNR (less than 1.91 of Rayleigh Distribution to SNR values down to zero) with the K distribution component and high SNR (greater than 1.91) with the homodyning "coherent" component. Thus, it allows for modeling media with small number of scatterers (low SNR) and media with a "coherent" component (high SNR). An application of this modeling technique would be image filtering for reducing speckle noise. The coherent signal parameter, s, relates to the structural signal, which is independent of the speckle noise. Therefore, estimates of s using the local moments could provide a statistical method for filtering ultrasound images.

ACKNOWLEDGMENTS

We thank Dr. Jian-yu Lu for providing us the phantoms for the study. Mr. Randall Kinnick's help in scanning the phantoms was invaluable in getting the job done with ease. We also thank Mr. Thomas Kinter for providing various programming functions and utilities which helped in the ease of writing the software for the computations. We thank Professor R. S. Bain for the freely distributed FORTRAN code, the NNES (Nonmonotonic Nonlinear Equation Solver) Library, which was used to construct the equation solver for the moments equations. This work was supported in part by grants CA 43920 and HL 41046 from National Institutes of Health.

REFERENCES

[1] Tuthill, T. A., Sperry, R. H., and Parker, K. J., "Deviation from Rayleigh statistics in ultrasonic speckle," *Ultrasonic Imaging* 10, 81–90 (1988).

[2] Wagner, R. F., Insana, M. F., and Brown, D. G., "Unified approach to the detection and classification of speckle texture in diagnostic ultrasound," *Optical Engineering* 25, 738–742 (1986).

[3] Insana, M. F., Wagner, R. F., Garra, B. S., Brown, D. G., and Shawker, T. H., "Analysis of ultrasound image texture via generalized Rician statistics," *Optical Engineering* 25, 743–748 (1986).

[4] Wagner, R. F., Insana, M. F., and Brown, D. G., "Statistical properties of radio-frequency and envelope-detected signals with applications to medical ultrasound," *J. Opt. Soc. Am.* 4, 910–922 (1987).

[5] Lizzi, F. L., Greenebaum, M., Feleppa, E. J., and Eldaum, M., "Theoretical framework for spectrum analysis in ultrasonic tissue characterization," *J. Acoust. Soc. Am.* 73, 1366–1373 (1983).

[6] Jacobs, E. M. G. P. and Thijssen, J. M., "A simulation study of echographic imaging of diffuse and stucturally scattering media," *Ultrasonic Imaging* 13, 316–333 (1991).

[7] Jakeman, E., "On the statistics of K-distributed noise," *J. Phys. A* 13, 31–48 (1980).

[8] Jakeman, E., "Speckle statistics with a small number of scatterers," *Optical Engineering* 23, 453–461 (1984).

[9] Weng, L., Reid, J. M., Shankar, P. M., and Soetanto, K., "Ultrasound speckle analysis based on the K-distribution," *J. Acoust. Soc. Am.* 89, 2992–2995 (1991).

[10] Shankar, P. M., Reid, J., Ortega, H., and Goldberg, B. B., "Use of non-Rayleigh statistics for the identification of tumors in ultrasonic B-scans of the breast," *IEEE Trans. Medical Imaging* 12, 687–692 (1993).

[11] Jakeman, E. and Tough, R., "Generalized K distribution: a statistical model for weak scattering," *J. Opt. Soc. Am.* 4, 1764–1772 (1987).

[12] Goodman, J. W., "Some fundamental properties of speckle," *J. Opt. Soc. Am.* 66, 1145–1150 (1976).

[13] Goodman, J. W., *Statistcal Optics* (John Wiley and Sons, New York, 1985).

[14] Rice, S. O., "Mathematical analysis of random noise," *Bell Syst. Tech. J.* 14, 46–158 (1945).

[15] Jakeman, E. and Pusey, P. N., "A model for non-Rayleigh sea echo," *IEEE Trans. Antennas Propagation* AP-24, 806–814 (1976).

[16] Molthen, R. C., Narayanan, V. M., Shankar, P. M., Reid, J. M., Genis, V., and Vergara-Dominguez, L., "Ultrasound echo evaluation by K-distribution," in *1993 IEEE Ultrasonics Symposium Proceedings*, pp. 957–960.

[17] Bain, R. S., "NNES user's manual," University of British Columbia, Vancouver BC, Canada, bain@gandolf.commerce.ubc.ca (1993).